https://doi.org/10.1016/j.apsusc.2020.147803

This is the Pre-Published Version.

Extending the near-infrared band-edge absorption spectrum of silicon by proximity to a 2D semiconductor

Valerio Apicella[a,b,1] , Teslim Ayinde Fasasi[a,1], Hon Fai Wong[c], Dennis C.W.Leung[c], Antonio Ruotolo[d]

[a] Department of Materials Science and Engineering, City University of Hong Kong, Kowloon, Hong Kong, China

[b] Department of Engineering, University of Sannio, Benevento 82100, Italy

[c] Department of Applied Physics, The Hong Kong Polytechnic University, Hum Hom, Hong Kong, China

[d] Department of Natural Sciences, Florida Polytechnic University, Lakeland, FL 33805-8531, USA

© 2020. This manuscript version is made available under the CC-BY-NC-ND 4.0 license http://creativecommons.org/licenses/by-nc-nd/4.0/.

Highlights

• The infrared absorbance of Si is enhanced by proximity to a 2D semiconductor.

• Spectroscopy measurements show a narrowing of the Si bandgap near the interface.

• Photo-induced Hall effect is used to estimate the increase of the photo-conversion efficiency.

• The effect could be exploited for photovoltaic applications after further investigations.

Keywords

2D semiconductorsTransition-metal dichalcogenidesPhoto-conversionBand-gap engineering

Abstract

Because of its low-cost, silicon is the standard material for photovoltaic conversion. Yet, its band-edge absorption spectrum is narrower than the spectrum of the solar radiation, which reduces its conversion efficiency. In this paper, it is shown that the spectrum of absorbance of silicon can be extended to longer wavelengths by proximity to a two-dimensional (2D) semiconductor. Photo-induced Hall effect, together with standard absorption spectroscopy, was employed to estimate the increase of photo-conversion efficiency of a 2D-platinum-diselenide/intrinsic-silicon heterostructure. The system shows a significantly higher absorption in the infrared as compared to the single films. Angle resolved X-ray Photoelectron Spectroscopy (XPS) confirm that a change of the band structure occurs in the silicon substrate at the interface between the two semiconductors. The results are interpreted in the framework of band-gap narrowing due to hole-confinement in the Si, induced by electron-confinement in the 2D film. This allows us to claim that the increase of photo-conversion efficiency in the Pt/$PtSe_2$/Si sample is due to an enhancement of the light absorbance of silicon near the interface. Possible application of the effect in photo-voltaic cells is discussed.

1. Introduction

The need for inexpensive renewable energy sources and the potentialities of harvesting the huge energy amount coming from the sun in a more efficient way, has been pushing both industry and research of last decades towards finding new solutions to increase the solar cells efficiency. Among the large variety of materials exploited in photovoltaics, silicon remains the most used one because of its abundance and its consequently very low-cost. Nevertheless, its band-gap of 1.12 eV represents one of the major issues limiting its performances in photovoltaic conversion [1], [2]. It sets the edge of the absorption spectrum at about 1107 nm [3]. As a consequence, the largest amount of the near-infrared solar spectrum content is lost and does not take part to the energy conversion process. Different solutions have been proposed in literature to enhance the absorption of the infrared light. The possibility of coupling more semiconductors in multi-gap [4], or multi-junction [5], tandem solar cells is an example. In particular, two or more solar cells with different absorption characteristics are series-connected together through tunnel junctions with the aim of covering a wider part of the solar spectrum. Recent examples of tandem solar cells make use of polymers [6] and organic cells [7].

In the same direction goes the exploitation of thin films to improve the infrared absorption [8]. First examples are given in [9], [10] where a $CuInGaSe_2$ and a low band-gap polymer were proposed, respectively. More recently, the usage of quantum dots [11], [12] and nanowires [13], [14] was proposed for infrared photovoltaics.

After graphene was discovered in 2004 [15], new possibilities arose in developing photovoltaic devices [16], [17], leading also to the usage of other two-dimensional (2D) materials [18]. Among the latter class of semiconductors, most promising for infrared absorption and detection seem to be the transition-metal dichalcogenides (TMDs) [19], [20], [21], [22], [23].

In this paper, a simple method to extend the near-infrared band-edge absorption spectrum of silicon (Si) is presented. In particular, 2D platinum diselenide ($PtSe_2$), a narrow band-gap TMD semiconductor, is exploited. As explained in the following, the large difference in band-gap between the two semiconductors results in an electron confinement in the 2D layer, which induces a hole confinement in the Si near the interface. The concentration of holes near the interface results in a narrowing of the optical band-gap and, therefore, an increase in both the absorbance efficiency and absorbance spectrum. The high resistivity of the intrinsic silicon favors the confinement of the hole-plasma near the interface. Photo-induced Hall effect [24], together with standard spectroscopy, allowed us to estimate the increase of photo-conversion efficiency. The heterostructure behaves as a single, engineered semiconductor with an overall increase of 20 times in photo-conversion efficiency, partially due to an increase of absorbance in the infrared range, which takes place near the interface in the Si, not in the 2D semiconductor. Our interpretation is supported by angle-resolved X-ray Photoelectron Spectroscopy (XPS) measurements, which confirm that a change of the band structure occurs in the Si near the interface.

2. Materials and methods

Materials information.

The two-dimensional semiconductor used in the present work is a two/three atomic layer platinum diselenide ($PtSe_2$), a transition-metal dichalcogenide which has been demonstrated to undergo a transition from metal to semiconductor by reducing its thickness from bulk to two-dimensional layers [25]. Samples films were purchased from *SixCarbon Technology (Shenzhen)*. The average thickness of the layer, as measured by atomic force microscopy (AFM), provided by

the supplier and available at www.6carbon.com, is 1.8 nm. The system of interest here is an 1×1 cm^2 $PtSe_2$/Si heterostructure, where the Si substrate was chosen to be intrinsic Si (i-Si) for reasons that will be explained in the following. An 1×1 cm^2 PtSe2/α-Al_2O_3 structure was used as reference in optical measurements, while two more reference samples, namely Pt/$PtSe_2$/α-Al_2O_3 and Pt/Si, were used as reference for photo-induced Hall measurements. The used wafer was device-quality, i-Si with a resistivity higher than 10000 Ωcm and a carrier density of 1.5×1010cm^{-3} at 300 K.

Samples preparation.

The purchased 2D films were grown by chemical vapor deposition on dedicated SiO_2/Si substrates, following the protocol detailed in Refs. [26], [27], before being transferred onto the specific substrate (Si or α-Al_2O_3) and annealed in vacuum at 150°C. While native oxide was chemically removed from the Si wafers, residues might exist due to the transfer process. Pt thin films for photo-induced Hall effect measurements were deposited thorough *Pulsed Laser Deposition (PLD)* method (laser energy: 300 mJ, frequency: 3 Hz, pulse width: 25 ns, deposition time: 180 s, pressure: 10-1 Torr).

Spectroscopy measurements.

The Raman spectroscopy measurements were carried out with a *WITec ALPHA300* (laser at 532 nm). A *PerkinElmer* spectrometer was used to perform the Fourier-transform infrared spectroscopy experiments. A *Thermo Scientific Nexsa XPS System* was used for XPS measurements.

Photo-induced Hall effect measurements.

Magnetic fields were applied through an *GMW 5403* electromagnet supplied by two *RS-PRO RSPD 3303C*. A halogen lamp *Halopar 30* by *Osram* was used as the light source and

an *FELH1250* edge-pass filter (long-pass wavelength at 1250 nm) by *ThorLabs* was exploited to cut the visible part. The open-circuit Hall voltage was measured by using a *Keithley 2182A* nanovoltmeter. Electric contacts to the samples were made by aluminum wire bondings.

3. Results

3.1. Raman spectroscopy

The measured Raman spectrum of the 2D film is shown in Fig. 1. The measurement was carried out on the PtSe2/α-Al_2O_3 sample, in order to avoid the high intensity signal from the Si. The spectrum is consistent with the one expected for the 2D semiconductor [28]. In particular, two main peaks at 176 cm^{-1} and 205 cm^{-1} and one with lower intensity at 229 cm^{-1} can be observed. The first two are assigned to E_g and A_{1g} modes, respectively. The third one corresponds to the overlapping of A_{2u} and E_u modes. As discussed in [28] the latter peak disappears for thickness of about 5 nm. Furthermore, the higher its relative intensity, with respect to the more prominent ones, the thinner the $PtSe_2$ layer. As a consequence, the Raman spectrum in Fig. 1 confirms the two-dimensional nature of the $PtSe_2$ layer under test.

3.2. Fourier transform infrared spectroscopy

In order to investigate how the proximity to the 2D semiconductor affects the optical behavior of the silicon substrate, *Fourier Transform Infrared* (FTIR) spectroscopy measurements were performed on the two samples and on the bare Si. In Fig. 2 one can see that in the near-infrared, beyond the Si band-gap (1107 nm), the absorbance of the $PtSe_2$/Si sample is more than twice that of Si and PtSe2/α-Al_2O_3 samples. An increase of absorbance in the PtSe2/α-Al_2O_3 sample at

longer wavelengths, which becomes dominant above 5000 nm (see Fig. S1 in Supplementary Material) can be ascribed to the absorbance of the sapphire substrate [29], [30], and is of no interest in the present framework.

The band-gap of the 2D semiconductor was estimated through the *Tauc* analysis [31] of the absorbance spectrum of the PtSe2/α-Al_2O_3 reference sample. The Tauc plot of the absorbance spectrum is shown in Fig. 3. The noise at low photon energies is due to the aforementioned absorbance of the sapphire for wavelengths longer than 5000 nm. Then, a clear change of slope is observed for photon energies near the expected band-gap value. The absorbance depends on the difference between photon energy and band-gap, as $(\alpha h\nu)1/n \propto (h\nu - Eg)$, where n=2 for indirect band-gap semiconductors [32], such as in the case of 2D $PtSe_2$ [33]. As a consequence, a bandgap Eg,2D=0.21 eV was estimated by using the intercept to the x–axis (see Fig. 3). This value is in agreement with other works [34], dealing with two-dimensional $PtSe_2$.

3.3. Photo-induced Hall effect measurements

Photo-induced Hall effect [24] offers the possibility to characterize the optical behavior of a semiconductor without flowing of a net-charge current. As will be discussed in the next section, this is important to exclude band-gap narrowing due to excitation and injection of high-density carriers through the 2D/Si interface [35]. Furthermore, it allows us to probe the optical properties of $PtSe_2$/Si near the interface, where the enhancement of the infrared absorption is expected to occur. The working principle is briefly explained in the following with the help of Fig. 4. A metal with high work-function, such as platinum (Pt) is deposited on the semiconductor or, in this case, on the semiconductor hetero-structure. The thickness of the metal is chosen in such a way that light can penetrate without significant attenuation for wavelengths as long as infrared

radiations. In this experiment the thickness of the Pt was 3 nm. The metal forms a Schottky barrier to the semiconductor (see Fig. S2 of Supplementary Material). As photons are converted into electron-hole pairs, while holes can easily be neutralized by electrons in the metal, electrons are confined near the interface, if the semiconductor is highly resistive. This results in a rounding-off of the barrier due to image force effect [36]. The reduction of the barrier potential allows electron to be injected into the metal, as schematically shown in Fig. 4a. If a magnetic field is applied in the sample plane, an open-circuit voltage appears that is transverse to the metal (Fig. 4b). At equilibrium, the current of the holes and the current of the electrons are equal and no net-current flows, while the current densities are not uniform because of the Lorentz's forces exerted on the carriers.

Fig. 5a shows the open-circuit voltage detected on the Pt/$PtSe_2$/Si when illuminated by a halogen lamp and for different values of the applied magnetic field. Fig. 5b shows the same measurement when a long-pass, infrared filter with cut-off wavelength of 1250 nm (which is safely longer than 1107 nm, i.e. the absorption spectrum of silicon), is placed in front of the sample. In both cases, the Hall voltage was normalized to the measured light intensity. One can clearly see that photo-conversion occurs in the near-infrared, in agreement with the FTIR measurements. In order to understand where absorption of infrared occurs, we prepared two additional reference samples, Pt/$PtSe_2$/α-Al_2O_3 and Pt/Si for photo-induced Hall effect. In Fig. 6a and Fig. 6b we compare the photo-induced Hall effect measured on the three samples at a fixed value of the magnetic field. In agreement with the FTIR measurements, absorption of infrared light is highly enhanced in the Pt/$PtSe_2$/Si heterostructure as compared to the case of single semiconductors. Furthermore, by dividing the intensities of voltages obtained in the full spectrum of the lamp (Fig. 6a) on the

$Pt/PtSe_2/Si$ and Pt/Si samples, an increase by a factor 20 of the measured open-circuit voltage is obtained.

It is also important to highlight that the sample with sapphire substrate does not respond at any wavelength (see Fig. 6). This allows us to claim that the increase of photo-conversion efficiency in the $Pt/PtSe_2/Si$ sample is due to an enhancement of the light absorbance of silicon near the interface, which is consistent with the increase of absorbance in the IR range, as detected by FTIR.

Finally, photo-induced Hall measurements with daylight blue and red filters were carried out and shown in Fig. S3 (see Supplementary Material). By comparing the relative intensities of the signals obtained over the two samples, it is straightforward to note that a shift in the absorbance peak to longer wavelengths is obtained in the $Pt/PtSe_2/Si$ sample with respect to the Pt/Si one. This demonstrates that the 20 times increase of the overall photo-conversion efficiency mainly occurs in the red and infrared wavelength range.

3.4. Angle-resolved X-ray photoelectron spectroscopy

Angle resolved X-ray photoelectron spectroscopy (AR-XPS) measurements were carried out on the $PtSe_2/Si$ sample at different angles. XPS spectra were recorded at 0, 30, 45, 60 and 75°. The full spectrum at 0° is shown in Fig. S4 (see Supplementary Material), while the Si peaks at all the angles are shown in Fig. 7. Measurements were also carried out on a bare-Si sample for comparison and are shown in Fig. S5 (Supplementary Material). In Fig. 7, one can clearly observe the presence of four peaks that are better resolved by Lorentzian deconvolution. The peak at higher binding energy (*Peak 1* in the figure) can be attributed to residues of SiO_2 [37] formed during the transfer process of the 2D material on the silicon substrate (as

explained in Section 2). In fact, this peak exists in the spectrum of bare, un-etched Si and disappears after etching in the XPS chamber (see Fig. S5). *Peaks 2* and *3* are the expected Si2p1/2 and Si2p3/2 peaks of Si [38]. Surprisingly, a forth peak can be resolved at lower binding energies that is not present in the XPS of bare Si. The intensity ratio between peak 4 and peak 3 is reported in Table 1, together with the intensity ratio between the Si peaks. Since the ratio between Si peaks is expected to be insensitive to the angle [38], its value is a good indication of the quality of the fittings. In the bottom-right panel of Fig. 7, we plot the Si2p core line center (defined as the midpoint of the peak positions of the Si2p1/2 and Si2p3/2 peaks). The dash line is the Si2p core line center estimated from the fitting of the XPS on bare Si). The error bar is taken as a half of the energy step used in the acquisition of the data (0.05 eV). A clear shift of the binding energy core level with increasing angle can be observed. As discussed in the following section, the presence of peak 4 and and the shift of the Si2p core line center with the angle suggest a change of the Si band-structure near the interface.

4. Discussion

The results presented in the previous section suggest a profound change of the band-structure of the Si near the interface on a mesoscopic scale. In particular, the increase of the absorption efficiency in the visible range and the extension of the absorption spectrum into the near infrared suggest an overall band-gap narrowing (BGN). Such a significant narrowing of the optical band-gap in Si can only be ascribed to the presence of high density of electron-hole pairs [39]. In brief, the band-gap is by definition the minimum energy required to generate an unbound electron-hole pair. The distance between the electron and the hole in the crystal is such that electrostatic attraction between the two particles can be neglected. On the contrary, excitons in a crystal can

be excited by providing smaller energy. An exciton is a quasiparticle in which an electron and a hole are attracted to each other by the electrostatic Coulomb force. The confinement of a high density of carriers favors conversion of photons into excitons. This requires less energy than that required to generate an unbound electron-hole pair. A reduction of the energy that a photon must possess to excite an electron-hole pair is equivalent to a reduction of the band-gap.

In traditional semiconductor hetero-junctions, the confinement of a high density of carriers can have three possible origins: i) heavy doping; ii) optical excitation of a large concentration of electron-hole pairs, usually through laser sources and iii) injection of high-density carriers through the interface of a biased junction, in which case the carriers, and therefore the BGN, are confined near the interface. Heavy doping in silicon has indeed been proven effective to extend its spectrum of absorption to the infrared [40], [41]. Of course, this possibility can here be excluded because the silicon used in this work is intrinsic. Excitation of a large concentration of electron-hole pairs can also be excluded, because in our experiment, unlike the Pt/$PtSe_2$/Si sample, the Pt/Si sample does not absorb infrared light, under the same experimental conditions. Last, injection of high-density carriers through the interface can be ruled out because the FTIR in Fig. 2 shows that a BGN of the heterostructure exists under no electrical bias. Besides, in photo-induced Hall effect, no net-current flows through the hetero-junction. One must conclude that, in our system, the confinement of high density of carriers near the interface in the Si is due to the proximity to the 2D film. On the other hand, not only the confinement of electrons in a 2D semiconductors has been proven to induce a change in the band-structure of the 2D [42], moreover, a bending of the valence band of a bulk semiconductor due to proximity to a 2D has been experimentally observed [43]. It is also important to highlight that this confinement of carriers cannot be considered as an effect of the metallic Pt on Si, since the infrared absorption of

the Pt/Si sample was significantly lower than the effect observed in the Pt-2D-Si system, as demonstrated with photo-induced Hall effect measurements.

Based on our experimental evidences, we propose the following, microscopic scenario. As the Si substrate is placed in intimate contact with the 2D semiconductor, electrons in the conduction band (CB) of the Si see a large density of energy states available across the interface and migrate (see Fig. 8a). On the contrary, holes from the 2D film see a large potential barrier and cannot migrate into the Si. The 2D behaves as a potential well for the electrons. As electrons are confined in a two/three atomic layers thick film, Coulomb interaction is not negligible and this results in a change of band-structure of the 2D [42], which is of secondary importance here, because the effect we observe is in the bulk semiconductor. From charge neutrality and from electrostatic considerations, a confinement of electrons in the 2D must induce a confinement of holes in the Si (see Fig. 8b), which, in agreement with Ref. [43], results in a bending of the VB. The bending of the VB can be detected by measuring the position of the Si 2p core level at different depths from the interface (see bottom-right panel of Fig. 7) [44].

We can give here an additional contribution to the understanding of this phenomenon. First, we can add that the bending of the band structure in the bulk semiconductor results in a reduction of the optical band-gap, which extends the range of absorption of the material. Our XPS measurements, together with the optical characterization, show that the band-structure of the silicon near the interface is significantly affected by the proximity of $PtSe_2$, with the changes in band structure not being limited to a VB bending. In fact, while a complete reconstruction of the band-structure of the semiconductor requires advanced spectroscopic techniques and should be the subject of a further investigation, in our XPS measurements, the low energy peak (*Peak 4*) can not be assigned to SiO_2 nor to Pt and Se in the 2D semiconductor. Peaks related to the latter

two elements are located at much lower binding energies and are shown in Figs. S6 and S7 (see Supplementary Material), respectively, for the case of 0°. Furthermore, the relative intensity between peaks 3 (Si2p3/2) and 4 decreases when the angle of the XPS increases, as shown in Table 1. This means that the contribution of the last peak increases near the interface between the bulk and the 2D semiconductors. As a consequence, the *Peak 4* is an additional evidence of a profound change of the band-structure of silicon, with an overall narrowing of the optical band-gap, due to proximity to a 2D.

Let us also point out that the effect we here observe should not be confused with the proximity effect due the penetration of electronic wavefunctions of one semiconductor into the other, which is purely quantum–mechanical and completely negligible in semiconductors.

Finally, let us speculate on how this effect could be employed in a photo-voltaic cell. If the intrinsic silicon substrate were to be replaced by doped Si to work as the active layer of a photo-voltaic cell, we predict the BGN to decrease as the doping level increases. This is because holes would not be confined near the interface, as charge could easily diffuse trough the bulk semiconductor. A structure of the kind p-2D/i-n++, where *p* and n++ represent a *p*-type and a highly doped *n*-type semiconductor, respectively, could yield a higher efficiency than a standard p-i-n structure, if an appropriate choice of the thickness of the *i*-Si is made. The thickness should be large enough to allow confinement and small enough not to increase significantly the overall resistance of the multilayer. An optimized choice of the thickness of the *i*-Si would yield an enhancement of photo-conversion efficiency in open-circuit conditions, which will be always lower than the experimental upper limit of 20, as measured in this study.

5. Conclusion

A simple method to enhance the near-infrared absorption of intrinsic silicon was proposed and discussed in this paper. In particular, a 2D $PtSe_2$/i-Si heterostructure was studied. It was shown that electron confinement in the 2D layer induces hole-confinement in the silicon substrate and near the interface. As a consequence, a change in the band structure of the bulk semiconductor near the interface is induced, leading to an overall narrowing of the optical band-gap. Furthermore, photo-induced Hall effect showed that an increase of photo-conversion efficiency by up to 20 times can be induced in the system, partially due to an extension of the absorbance spectrum to the infrared. The possibility of using such a strategy in solar cells technology was preliminarily discussed, too, and will be the subject of future works.

CRediT authorship contribution statement

AR designed and coordinated the experiment. TAF prepared the samples. VA and TAF performed the structural and magneto-optical characterization of the samples. VA and AR prepared the manuscript. HFW and DCWL carried out the XPS measurements. All authors edited and commented on the manuscript.

Declaration of Competing Interest

The authors declare that they have no known competing financial interests or personal relationships that could have appeared to influence the work reported in this paper.

Ackowledgement

The work described in this paper was partially supported by a grant from Florida Polytechnic University (Grant No. GR-2000026).

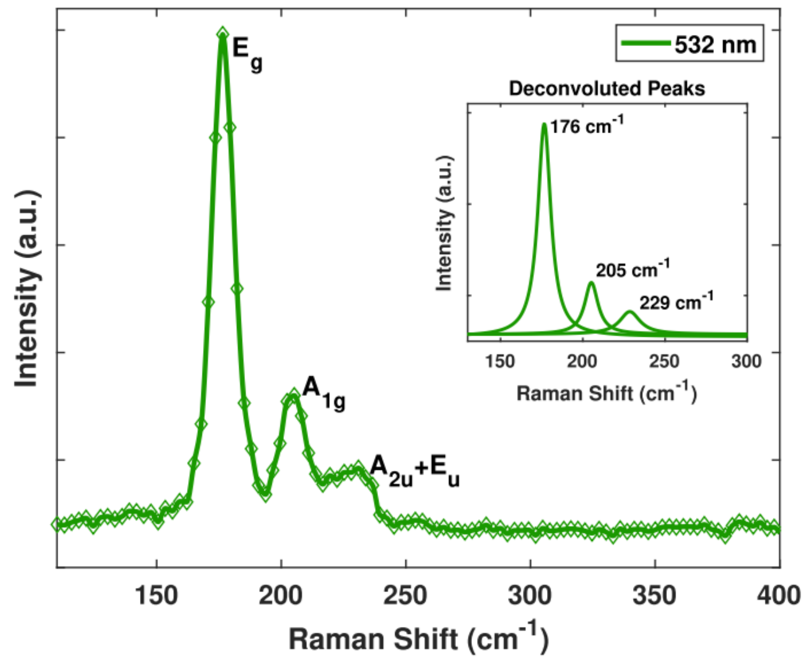

Fig. 1. Raman spectrum of the 2D PtSe2 sample on the sapphire substrate at 532 nm laser. The deconvoluted peaks are shown in the inset.

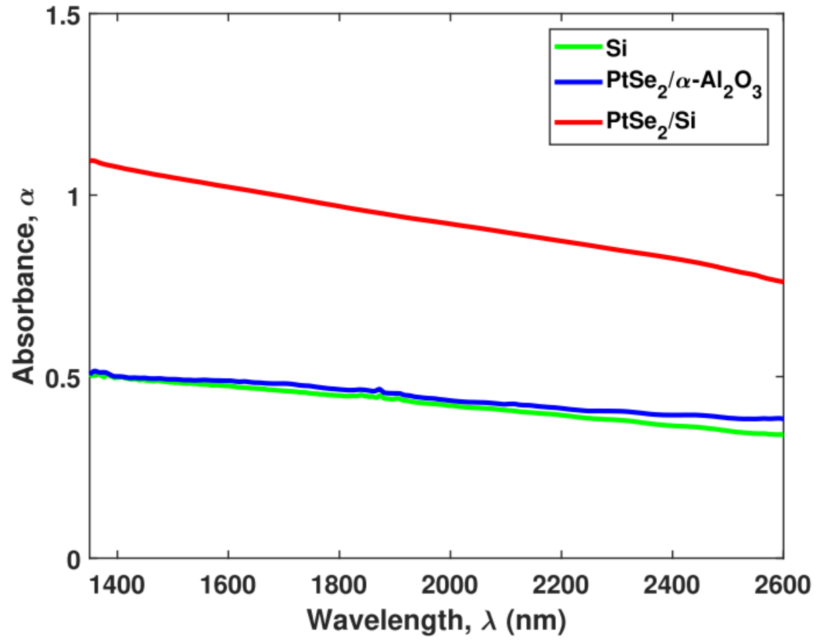

Fig. 2. FTIR absorbance spectrum of PtSe2/α-Al_2O_3 and $PtSe_2$/Si. The measured spectrum of the bare Si is shown for comparison.

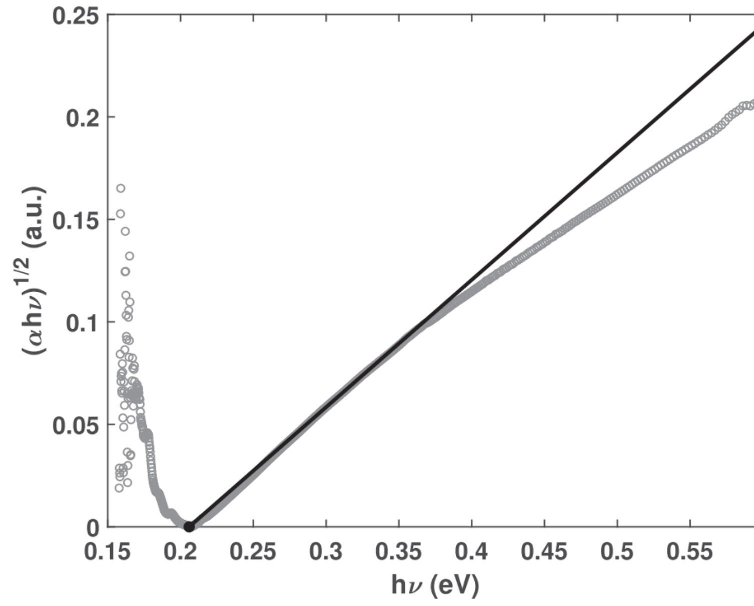

Fig. 3. Tauc plot calculated from the FTIR absorbance spectrum of the 2D $PtSe_2$ sample on the sapphire substrate. The band-gap of the 2D layer is estimated to be approximately equal to 0.21 eV.

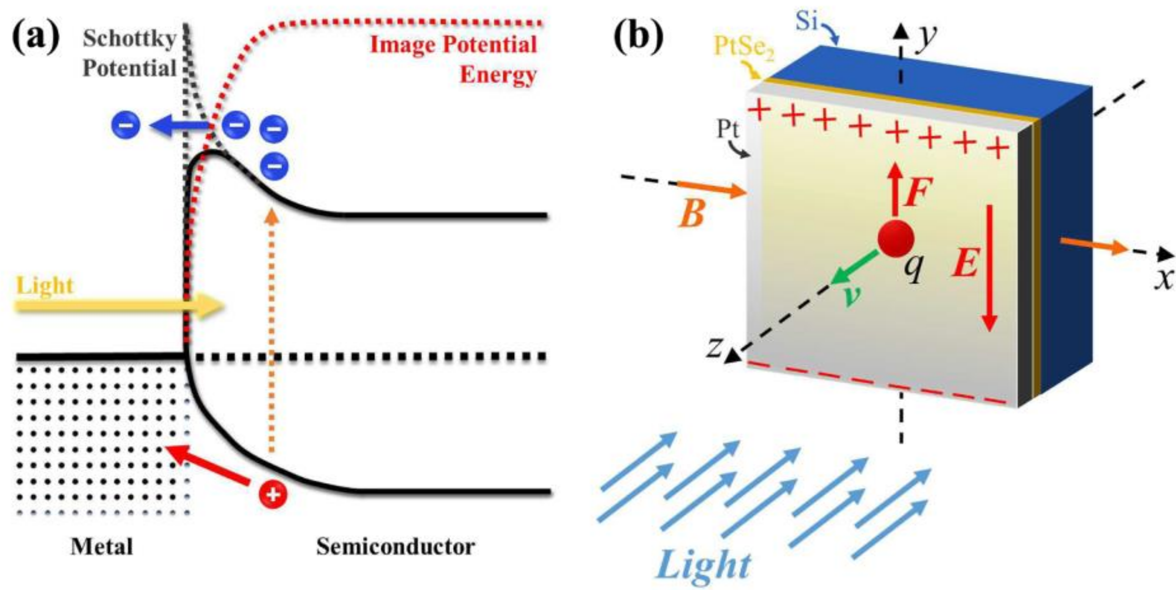

Fig. 4. Photo-induced Hall effect working principle: (a) barrier potential rounding-off due to image force effect; (b) photo-induced Hall voltage generation in the Pt/$PtSe_2$/Si sample.

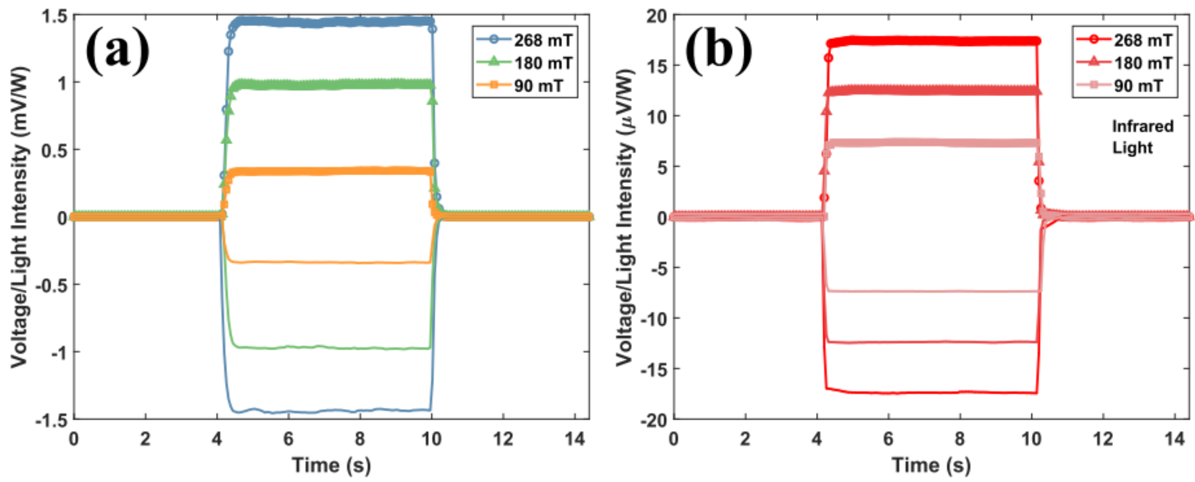

Fig. 5. Photo-induced Hall effect measurements on the Pt/$PtSe_2$/Si sample in the full halogen lamp spectrum (a) and infrared light (b). Both positive and negative magnetic fields were applied and represented with marked and unmarked lines, respectively.

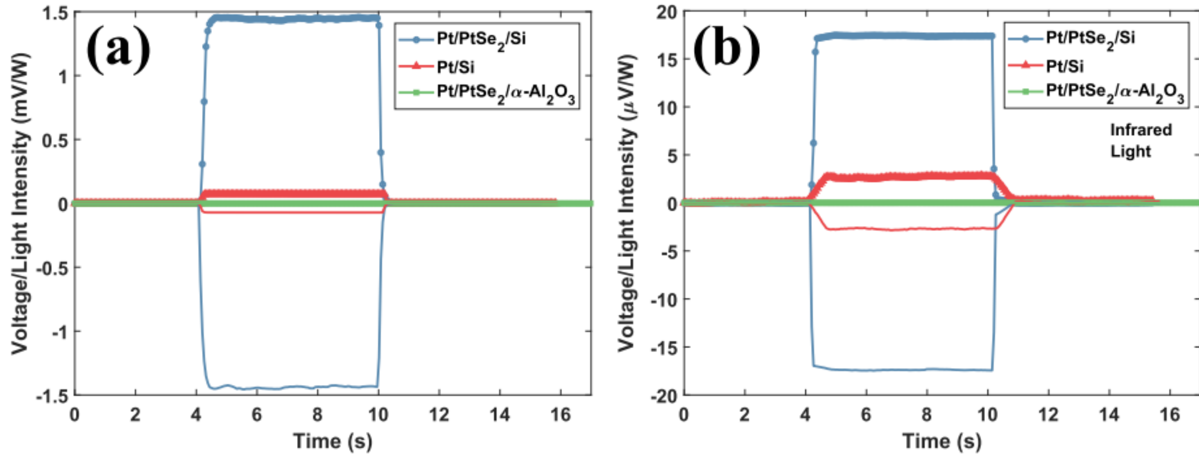

Fig. 6. Comparison of photo-Hall effect for $Pt/PtSe_2/Si$, Pt/Si and $Pt/PtSe_2/\alpha\text{-}Al_2O_3$ in full halogen spectrum (a) and infrared light (b). Both positive and negative magnetic fields with 268 mT amplitude were applied and represented with marked and unmarked lines, respectively.

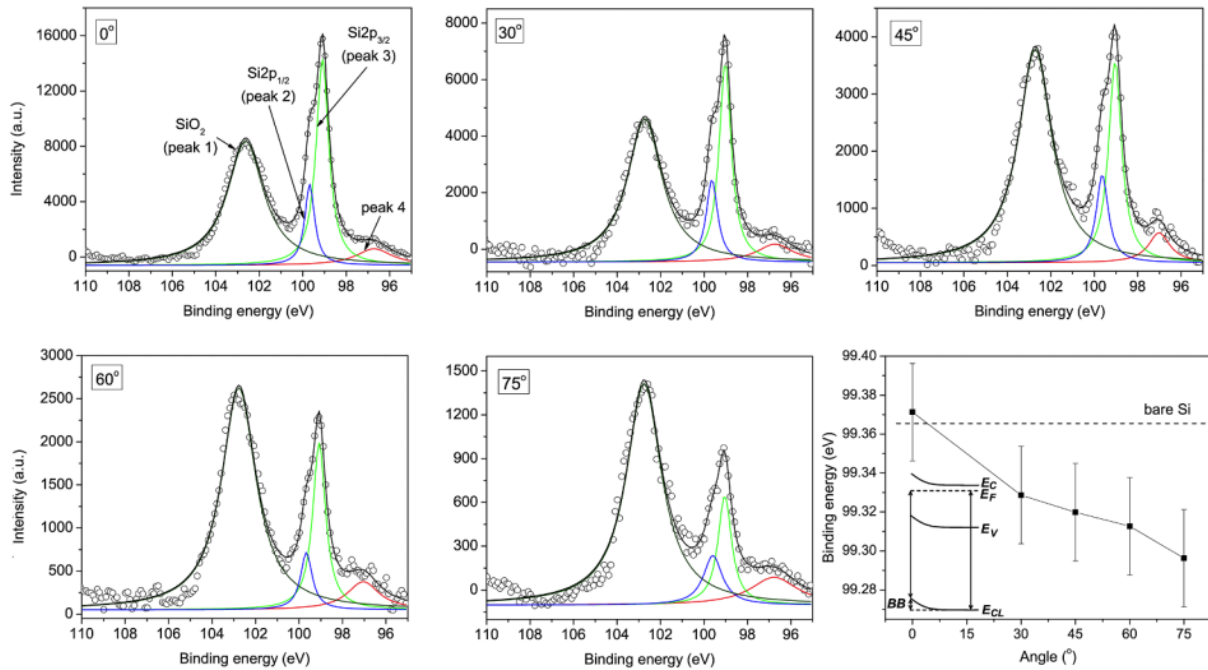

Fig. 7. Silicon XPS peaks (dots: measured data; color lines: deconvoluted peaks; black line: convolution) measured at different angles. The bottom-right panel shows the Si2p core line center as a function of the angle. The inset is a sketch of the core-line bending due to the bend bending (BB) near the interface.

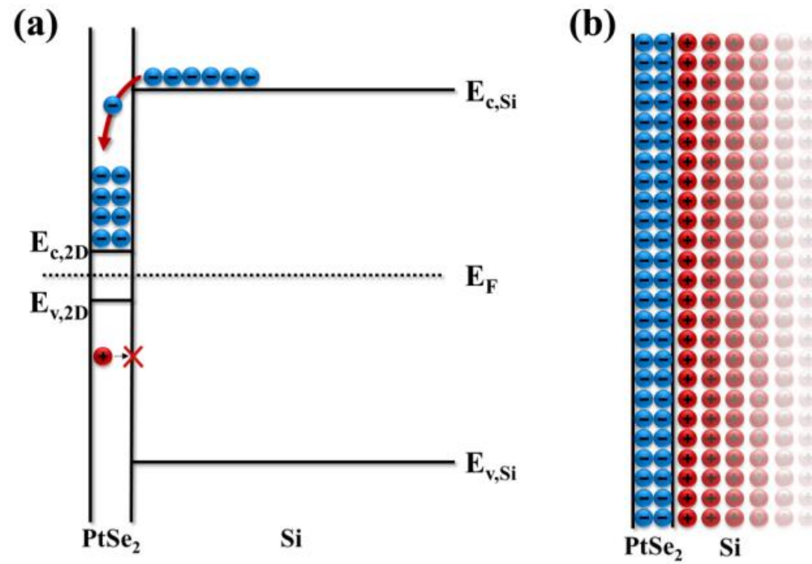

Fig. 8. Schematic explanation of the band-gap narrowing near the interface: (a) electron in the Si conduction band migrate to the 2D semiconductor; (b) an electron-hole plasma appears near the interface due to the electron confinement in the 2D layer.

Table 1. Ratios between intensities of peak 3 (Si2p3/2) and peak 4 and intensities of Si peaks at the considered angles.

	0°	30°	45°	60°	75°
$\frac{\text{Peak3}}{\text{Peak4}}$	12.5	11.2	6.7	5.9	3.9
$\frac{\text{Peak3}}{\text{Peak2}}$	2.5	2.4	2.3	2.7	2.2

Reference

[1] T. Tiedje, E. Yablonovitch, G.D. Cody, B.G. Brooks, Limiting efficiency of silicon solar cells, IEEE Trans. Electron Dev. 31 (5) (1984) 711–716.

[2] A. Richter, M. Hermle, S.W. Glunz, Reassessment of the limiting efficiency for crystalline silicon solar cells, IEEE J. Photovolt. 3 (4) (2013) 1184–1191.

[3] A. Shalav, B. Richards, T. Trupke, K. Krämer, H.-U. Güdel, Application of NaYF4: Er3+ up-converting phosphors for enhanced near-infrared silicon solar cell response, Appl. Phys. Lett. 86 (1) (2005) 013505.

[4] A. Marti, G.L. Araújo, Limiting efficiencies for photovoltaic energy conversion in multigap systems, Sol. Energy Mater. Sol. Cells 43 (2) (1996) 203–222.

[5] I. Tobias, A. Luque, Ideal efficiency of monolithic, series-connected multijunction solar cells, Prog. Photovoltaics Res. Appl. 10 (5) (2002) 323–329.

[6] J. You, L. Dou, K. Yoshimura, T. Kato, K. Ohya, T. Moriarty, K. Emery, C.-C. Chen, J. Gao, G. Li, et al., A polymer tandem solar cell with 10.6% power conversion efficiency, Nat. Commun. 4 (2013) 1446.

[7] L. Meng, Y. Zhang, X. Wan, C. Li, X. Zhang, Y. Wang, X. Ke, Z. Xiao, L. Ding, R. Xia, et al., Organic and solution-processed tandem solar cells with 17.3% efficiency, Science 361 (6407) (2018) 1094–1098.

[8] T.D. Lee, A.U. Ebong, A review of thin film solar cell technologies and challenges, Renewable Sustainable Energy Rev. 70 (2017) 1286–1297.

[9] W. Devaney, W. Chen, J. Stewart, R. Mickelsen, Structure and properties of high efficiency ZnO/CdZnS/CuInGaSe/sub 2/solar cells, IEEE Trans. Electron Dev. 37 (2) (1990) 428–433.

[10] C.J. Brabec, C. Winder, N.S. Sariciftci, J.C. Hummelen, A. Dhanabalan, P.A. van Hal, R.A. Janssen, A low-bandgap semiconducting polymer for photovoltaic devices and infrared emitting diodes, Adv. Funct. Mater. 12 (10) (2002) 709–712.

[11] X. Yan, X. Cui, B. Li, L.-S. Li, Large, solution-processable graphene quantum dots as light absorbers for photovoltaics, Nano Lett. 10 (5) (2010) 1869–1873.

[12] J. Tang, E.H. Sargent, Infrared colloidal quantum dots for photovoltaics: fundamentals and recent progress, Adv. Mater. 23 (1) (2011) 12–29.

[13] C. Lin, M.L. Povinelli, Optical absorption enhancement in silicon nanowire arrays with a large lattice constant for photovoltaic applications, Opt. Exp. 17 (22) (2009) 19371–19381.

[14] M.D. Kelzenberg, S.W. Boettcher, J.A. Petykiewicz, D.B. Turner-Evans, M.C. Putnam, E.L. Warren, J.M. Spurgeon, R.M. Briggs, N.S. Lewis, H.A. Atwater, Enhanced absorption and carrier collection in Si wire arrays for photovoltaic applications, Nat. Mater. 9 (3) (2010) 239.

[15] K.S. Novoselov, A.K. Geim, S.V. Morozov, D. Jiang, Y. Zhang, S.V. Dubonos, I.V. Grigorieva, A.A. Firsov, Electric field effect in atomically thin carbon films, Science 306 (5696) (2004) 666–669.

[16] Z. Liu, Q. Liu, Y. Huang, Y. Ma, S. Yin, X. Zhang, W. Sun, Y. Chen, Organic photovoltaic devices based on a novel acceptor material: graphene, Adv. Mater. 20 (20) (2008) 3924–3930.

[17] C.-T. Chien, P. Hiralal, D.-Y. Wang, I.-S. Huang, C.-C. Chen, C.-W. Chen, G.A. Amaratunga, Graphene-based integrated photovoltaic energy harvesting/storage device, Small 11 (24) (2015) 2929–2937.

[18] Z. Liu, S.P. Lau, F. Yan, Functionalized graphene and other two-dimensional materials for photovoltaic devices: device design and processing, Chem. Soc. Rev. 44 (15) (2015) 5638–5679.

[19] Q.H. Wang, K. Kalantar-Zadeh, A. Kis, J.N. Coleman, M.S. Strano, Electronics and optoelectronics of two-dimensional transition metal dichalcogenides, Nat. Nanotechnol. 7 (11) (2012) 699.

[20] M. Bernardi, M. Palummo, J.C. Grossman, Extraordinary sunlight absorption and one nanometer thick photovoltaics using two-dimensional monolayer materials, Nano Lett. 13 (8) (2013) 3664–3670.

[21] D. Jariwala, V.K. Sangwan, L.J. Lauhon, T.J. Marks, M.C. Hersam, Emerging device applications for semiconducting two-dimensional transition metal dichalcogenides, ACS Nano 8 (2) (2014) 1102–1120.

[22] K.F. Mak, J. Shan, Photonics and optoelectronics of 2d semiconductor transition metal dichalcogenides, Nat. Photonics 10 (4) (2016) 216.

[23] C.L. Tan, H. Mohseni, Emerging technologies for high performance infrared detectors, Nanophotonics 7 (1) (2018) 169–197.

[24] D. Li, A. Ruotolo, Photo-induced hall effect in metals, Sci. Rep. 8 (1) (2018) 4372.

[25] A. Ciarrocchi, A. Avsar, D. Ovchinnikov, A. Kis, Thickness-modulated metal-tosemiconductor transformation in a transition metal dichalcogenide, Nat. Commun. 9 (1) (2018) 919.

[26] Y. Xue, Y. Zhang, Y. Liu, H. Liu, J. Song, J. Sophia, J. Liu, Z. Xu, Q. Xu, Z. Wang, J. Zheng, Y. Liu, S. Li, Q. Bao, Scalable production of a few-layer mos2/ws2 vertical heterojunction array and its application for photodetectors, ACS Nano 10 (2016) 573–580.

[27] J. Yuan, T. Sun, Z. Hu, W. Yu, W. Ma, K. Zhang, B. Sun, S.P. Lau, Q. Bao, S. Lin, S. Li,

Wafer-scale fabrication of two-dimensional pts2/ptse2 heterojunctions for efficient and broad band photodetection, ACS App. Mater. Inter. 10 (2018) 40614–40622.

[28] M. O'Brien, N. McEvoy, C. Motta, J.-Y. Zheng, N.C. Berner, J. Kotakoski, K. Elibol, T.J. Pennycook, J.C. Meyer, C. Yim, et al., Raman characterization of platinum diselenide thin films, 2D Mater. 3 (2) (2016) 021004.

[29] M.E. Thomas, R.I. Joseph, W.J. Tropf, Infrared transmission properties of sapphire, spinel, yttria, and alon as a function of temperature and frequency, Appl. Opt. 27 (2) (1988) 239–245.

[30] M.A. Druy, L. Elandjian, W.A. Stevenson, R.D. Driver, G.M. Leskowitz, L.E. Curtiss, Fourier transform infrared (ftir) fiber optic monitoring of composites during cure in an autoclave, in: Fiber Optic Smart Structures and Skins II, Vol. 1170, International Society for Optics and Photonics, 1990, pp. 150–160.

[31] J. Tauc, R. Grigorovici, A. Vancu, Optical properties and electronic structure of amorphous germanium, Phys. Status Solidi B 15 (2) (1966) 627–637.

[32] B.D. Viezbicke, S. Patel, B.E. Davis, D.P. Birnie III, Evaluation of the tauc method for optical absorption edge determination: ZnO thin films as a model system, Phys. Status Solidi B 252 (8) (2015) 1700–1710.

[33] A. Kandemir, B. Akbali, Z. Kahraman, S. Badalov, M. Ozcan, F. İyikanat, H. Sahin, Structural, electronic and phononic properties of ptse2: From monolayer to bulk, Semicond. Sci. Technol. 33 (8) (2018) 085002.

[34] Y. Wang, L. Li, W. Yao, S. Song, J. Sun, J. Pan, X. Ren, C. Li, E. Okunishi, Y.-Q. Wang, et al., Monolayer ptse2, a new semiconducting transition-metal-dichalcogenide, epitaxially grown by direct selenization of pt, Nano Lett. 15 (6) (2015) 4013–4018.

[35] J.A. del Alamo, R.M. Swanson, Modelling of minority-carrier transport in heavily doped silicon emitters, Solid-State Electron. 30 (11) (1987) 1127–1136.

[36] C. Chang, S. Sze, Carrier transport across metal-semiconductor barriers, Solid-State Electron. 13 (6) (1970) 727–740.

[37] C.D. Wagner, W.M. Riggs, L.E. Davis, J.F. Moulder, G.E. Muilenberg, Handbook of X-ray Photoelectron Spectroscopy, Perkin-Elmer Corporation, 1979.

[38] G. Cerofolini, C. Galati, L. Renna, Si 2p xps spectrum of the hydrogen-terminated (100) surface of device-quality silicon, Surf. Interface Anal. 35 (12) (2003) 968–973.

[39] C. Persson, U. Lindefelt, B. Sernelius, Plasma-induced band edge shifts in 3C-, 2H-, 4H-, 6H–SiC and Si, Solid-State Electron. 44 (3) (2000) 471–476.

[40] M. Balkanski, A. Aziza, E. Amzallag, Infrared absorption in heavily doped n-type Si, Phys. Status Solidi B 31 (1) (1969) 323–330.

[41] P. Schmid, Optical absorption in heavily doped silicon, Phys. Rev. B 23 (10) (1981) 5531.

[42] N. Alidoust, G. Bian, S.-Y. Xu, R. Sankar, M. Neupane, C. Liu, I. Belopolski, D.-X. Qu, J.D. Denlinger, F.-C. Chou, et al., Observation of monolayer valence band spin-orbit effect and induced quantum well states in MoX2, Nat. Commun. 5 (2014) 4673.

[43] A. Molle, A. Lamperti, D. Rotta, M. Fanciulli, E. Cinquanta, C. Grazianetti, Electron confinement at the Si/MoS2 heterosheet interface, Adv. Mater. Interfaces 3 (10) (2016) 1500619.

[44] E.A. Kraut, G.R.W., J.R. Waldrop, S.P. Kowalczyk, Semiconductor core-level to valence-band maximum binding-energy differences: Precise determination by x-ray photoelectron spectroscopy, Phys. Rev. B 28 (4) (1983) 1965.